ELSEVIER

Journal of Nuclear Materials 306 (2002) 126–133

journal of nuclear materials

www.elsevier.com/locate/jnucmat

Characterization of hot deformation behaviour of Zr–2.5Nb in β phase

R. Kapoor *, J.K. Chakravartty

Materials Science Division, Bhabha Atomic Research Centre, Trombay, Mumbai 400 085, India

Received 13 June 2002; accepted 9 September 2002

Abstract

Hot deformation characteristics of β Zr–2.5wt%Nb in the temperature range 1225–1425 K and in the constant true strain rate range of 0.002–10 s^{-1} were studied by uniaxial compression testing in vacuum. A processing map using the strain rate sensitivity parameter was developed for β Zr–2.5Nb on the basis of flow stress data as a function of temperature and strain rate for a given strain. A domain of high strain rate sensitivity of 0.5 at 1375 K and 0.002 s^{-1}, was obtained and the grain size in this domain was large and equiaxed, suggesting the occurrence of large grain superplasticity. Thermal activation analysis was employed to determine the experimental activation volume and enthalpy, from which it was suggested that the rate controlling mechanism involved the movement of dislocation jogs. A comparison of Zr–2.5Nb with Zr in β phase suggested that Nb shifts the domain peak to higher temperatures.

1. Introduction

Zirconium alloyed with 2.5wt% niobium (Zr–2.5Nb) is used as a pressure tube material in nuclear reactors. This possesses better strength, greater creep resistance and a lower rate of hydrogen uptake as compared to Zircaloy-2 under similar service conditions. Since this alloy is used in thin tubular form, considerable mechanical processing is involved in its manufacture, such as two stages of hot working following the melting stage, a few steps of cold working, annealing, and finally a cold working step for achieving desired strength, suitable microstructure and dimensional tolerance. Amongst these steps, hot working in the form of forging and extrusion is very important, as in addition to breaking the cast microstructure and shaping the ingot, this step is responsible for providing a chemically homogeneous product with a suitable microstructure for subsequent processing. It may thus be beneficial to hot work this material in the β phase field because of higher diffusion rates of alloying elements and lower flow stresses. In order to design and optimize the hot working processes of Zr–2.5Nb, it is therefore necessary to evaluate its high temperature deformation behaviour. Previous studies on the high temperature deformation behaviour of zirconium and zirconium base alloys, in the α and the $(\alpha+\beta)$ phase, were primarily aimed at either identifying the rate controlling mechanisms or optimizing the hot working parameters [1–10]. However, it appears that hot deformation behaviour of zirconium alloys in the β phase field has received very little attention [11–13]. As regards the effect of alloying addition on the deformation characteristics, it has been observed that α stabilizers have little effect on the deformation behaviour of the hcp α phase, while β stabilizers alter the deformation characteristics of the bcc β phase dramatically [6,7]. For example, the addition of Nb lowers the strain rate required for dynamic recrystallization by two orders of magnitude as compared to that of unalloyed Zr [10]. A previous investigation, conducted on commercially pure zirconium, has found large grain superplasticity in the

* Corresponding author. Tel.: +91-22 559 3816; fax: +91-22 5505 151.

E-mail address: rkapoor@magnum.barc.ernet.in (R. Kapoor).

0022-3115/02/$ - see front matter
PII: S0022-3115(02)01290-4

1200–1330 K temperature range and at strain rates lower than 0.1 s^{-1} [13].

The aim of the present investigation was to study the hot deformation characteristics of Zr–2.5wt%Nb alloy with a view to optimize its hot workability in the β phase field, and to identify the high temperature processes that occur dynamically. A brief comparison of β Zr–2.5Nb with βZr from a previous study, was done with a view to bring out the effect of Nb addition.

In this investigation, the hot working characteristics are studied using the approach of processing maps in the format of dynamic materials modeling techniques [14–17]. In these techniques, the strain rate and temperature variation of flow stress are considered, and the strain rate sensitivity is mapped as a function of both temperature and strain rate. In addition, regimes of stable flow are identified.

2. Experimental

The starting Zr–2.5wt%Nb (called as Zr–2.5Nb) material was obtained in the form of an extruded tube, the chemical analysis of which is given Table 1. Cylindrical specimens of 5 mm diameter and 7 mm height were machined such that the compression axis of the specimens was along the extrusion direction. Hot compression tests were conducted under 5×10^{-5} mbar (5×10^{-3} Pa) vacuum using BAHR-DIL805 deformation dilatometer. The α to β transformation of Zr–2.5Nb used in this investigation was established to be 1200 K, carried out by monitoring the change of length vs. temperature using a heating rate of 3 K s^{-1} in this dilatometer. Hence in this investigation all tests were performed at temperatures greater that 1200 K. The samples were heated at 3 K s^{-1} to six different temperatures in the range 1225–1425 K and deformed at constant true strain rates of 0.002–10 s^{-1}. A thermocouple was spot-welded on to the sample and the temperature was controlled within ±1 °C. The specimens were compressed to about half their height and cooled rapidly in situ. The deformed specimens were sectioned along the compression axis and prepared for metallographic examination using standard techniques.

From the load–displacement data obtained by compression tests, true stress (σ) – true plastic strain (ε) curves were generated and the flow stresses were corrected for adiabatic temperature rise for tests carried out at 1 s^{-1} and above. The measured stresses were also corrected for shear modulus variation (μ) with temperature (T) of β Zr data as taken from Padel and Groff [18]. This μ vs. T data was fitted to a second-order polynomial as shown below.

$$\frac{\mu(T)}{\mu_0} = -3.75 \times 10^{-7} T^2 + 2.15 \times 10^{-4} T + 1.24 = \mu'. \tag{1}$$

Here μ_0 is the shear modulus at the transformation temperature, and μ' is the functional temperature dependence of shear modulus. Thus σ/μ' is the stress corrected for the temperature dependence of the shear modulus. The variation of flow stress (σ) with temperature (T) and strain rate ($\dot{\varepsilon}$) was obtained from the $\sigma - \varepsilon$ curves at different temperatures and strain rates. A cubic polynomial function was fitted to $\log(\sigma/\mu') - \log(\dot{\varepsilon})$ and $\sigma/\mu' - 1/T$ data, and the strain rate sensitivity (m) calculated as

$$m = \left.\frac{\partial \ln(\sigma/\mu')}{\partial \ln \dot{\varepsilon}}\right|_T. \tag{2}$$

It is generally believed that the motion of dislocations involved in plastic deformation is thermally activated and the shear strain rate ($\dot{\gamma}$) and temperature (T) are related through the general Arrhenius type equation,

$$\dot{\gamma} = \dot{\gamma}_0 \exp\left(\frac{-\Delta G}{kT}\right). \tag{3}$$

Here ΔG is the activation free energy of the movement of the rate controlling species over a barrier, $\dot{\gamma}_0$ is the pre-exponential strain rate factor, and k is the Boltzmann constant. According to the thermally activated deformation theory, the activation volume (V) and the activation enthalpy (ΔH) can be represented as [19,20],

$$V = \left.\frac{-\partial \Delta G}{\partial \tau}\right|_T, \tag{4a}$$

$$\Delta H = \left.\frac{-\partial(\Delta G/kT)}{\partial(1/kT)}\right|_\tau. \tag{4b}$$

If the variation of $\dot{\gamma}_0$ with τ and T is neglected, then the experimental activation enthalpy and experimental activation volume can be obtained. Here the shear stress τ, and shear strain rate $\dot{\gamma}$, are used. It is assumed that the corresponding macroscopic quantities, the uniaxial stress σ, and macroscopic strain rate $\dot{\varepsilon}$, will also be related in a manner similar to τ and $\dot{\gamma}$. Thus from Eqs. (3), (4a) and (4b), and using σ and $\dot{\varepsilon}$ instead of τ and $\dot{\gamma}$, the experimental activation volume (V_{ex}), and the experimental activation enthalpy (ΔH_{ex}) can be expressed as [20]

Table 1
Chemical composition of the alloy (wt%)

Nb	Fe	O (ppm)	Other impurities	Zr
2.4–2.6	0.08–0.1	1000–1200	< 800 ppm	Balance

$$V_{ex} = kT \left. \frac{\partial \ln \dot{\varepsilon}}{\partial(\sigma/\mu')} \right|_T, \tag{5a}$$

$$\Delta H_{ex} = \left. \frac{-\partial \ln \dot{\varepsilon}}{\partial(1/RT)} \right|_{\sigma/\mu'} = -RT^2 \left. \frac{\partial \ln \dot{\varepsilon}}{\partial \ln(\sigma/\mu')} \right|_T \left. \frac{\partial \ln(\sigma/\mu')}{\partial T} \right|_{\dot{\varepsilon}}. \tag{5b}$$

In the present study, V_{ex} and ΔH_{ex} were calculated from the interpolated values of σ/μ' by taking the appropriate derivatives as in Eqs. (5a) and (5b).

The m values, obtained from Eq. (2), as a function of strain rate and temperature, were recorded as a 3D map, which was then reduced to an iso-strain rate sensitivity contour map in the temperature–strain rate plane. In addition to the strain rate sensitivity plot, the regimes of stable flow were identified using the following conditions [16,17]:

$$m \geqslant 0, \tag{6a}$$

$$-\frac{\partial m}{\partial \ln \dot{\varepsilon}} \geqslant 0, \tag{6b}$$

$$-\left(\frac{T}{\sigma}\frac{\partial \sigma}{\partial T} + 1\right) \geqslant 0, \tag{6c}$$

$$\frac{\partial m}{\partial T} \geqslant 0. \tag{6d}$$

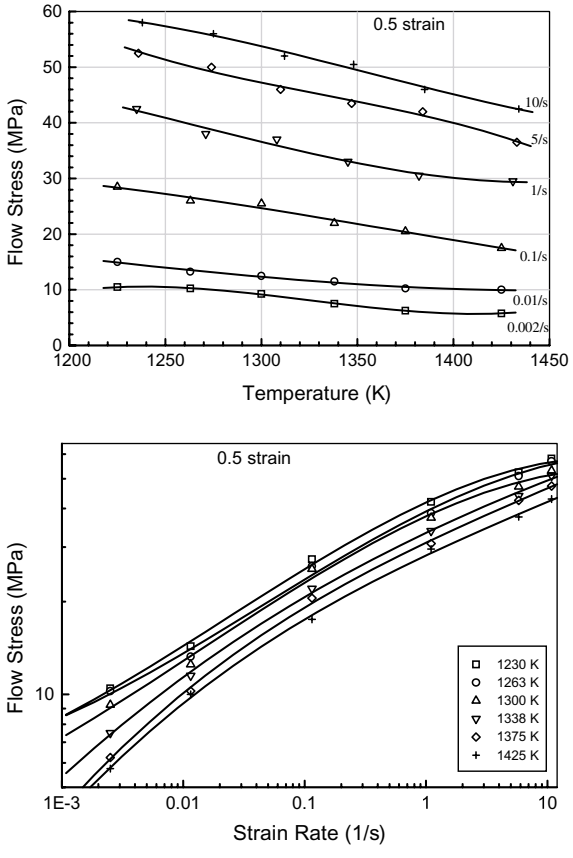

Fig. 1. (a) Flow stress vs. temperature and (b) log flow stress vs. log strain rate at 0.5 true strain.

3. Results

3.1. Flow behaviour and processing maps

Fig. 1 summarizes the dependence of the flow stress on temperature and strain rate. The flow stress increases with decreasing temperature and increasing strain rate. The magnitude of the slope of the σ–T curve increases with increasing $\dot{\varepsilon}$, as seen in Fig. 1(a). At lower strain rates, the slope of the $\log(\sigma/\mu') - \log(\dot{\varepsilon})$ increases with increasing temperature, as seen in Fig. 1(b). While at lower temperatures (< 1300 K) the rate of change of stress with strain rate appears to be flatter over the entire strain rate range, at higher temperatures the rate is higher particularly at lower strain rates. These changes will have considerable effect on the strain rate sensitivity and its variation with temperature and strain rate. The variations of strain rate sensitivity with strain rate and temperature are recorded in Fig. 2. It is seen that strain rate sensitivity varies gradually with strain rate and very little with temperature for strain rates greater than 0.01 s^{-1} (Fig. 2(a)). The strain rate sensitivity reaches a maximum of 0.5 at a temperature of 1375 K and at a strain rate of 2.5×10^{-2} s^{-1} (Fig. 2(b)). These variations are better seen in the form of iso-strain rate sensitivity contour plots on a frame of strain rate and temperature. Fig. 3 shows such a plot at two strains 0.2 and 0.5, with the numbers representing the m values. It is noted that the maps at different strains are essentially similar, exhibiting a single domain located in the strain rate range 2×10^{-3} to 3×10^{-2} s^{-1} and temperature range of 1280–1425 K. For the strain of 0.5, the instability domain [1] (hatched area) is superimposed on the m contour map. A peak strain rate sensitivity of 0.5 is obtained at 1375 K and 2×10^{-3} s^{-1}.

3.2. Activation volume and activation energy

In order to understand the high temperature processes that occur dynamically, thermal activation anal-

[1] Eqs. (6a)–(6d) are the conditions for stable flow. The flow is considered unstable if any of these conditions are not satisfied.

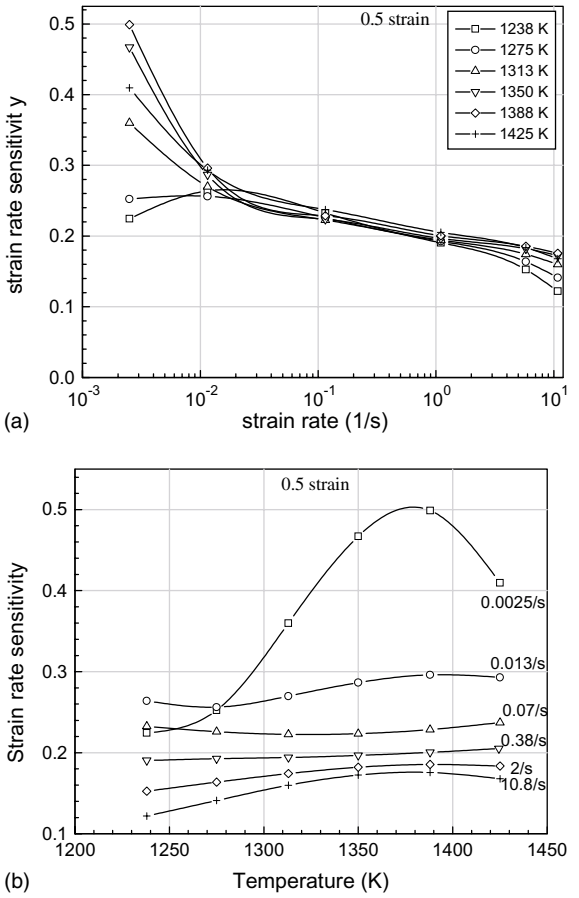

Fig. 2. Plot of (a) m vs. strain rate at different temperatures; (b) m vs. temperature at different strain rates, for 0.5 strain.

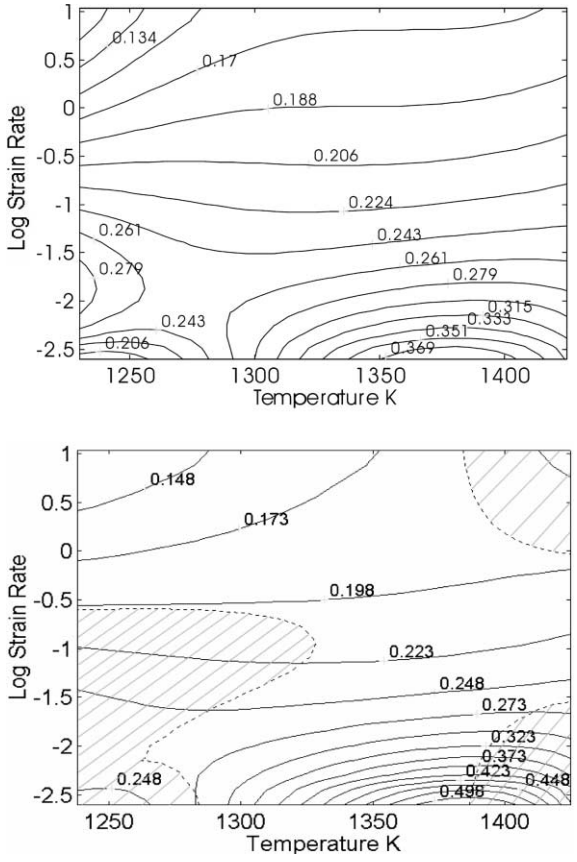

Fig. 3. Contour plot of strain rate sensitivity at (a) 0.2 and (b) 0.5.

ysis has been carried out using the standard method described earlier. In this context two parameters namely activation volume and activation enthalpy are of interest. Activation volume is a thermodynamic parameter quantifying the volume associated with the movement of the rate controlling species, thereby providing an idea of deformation mechanism. In addition, a given rate controlling mechanism has a characteristic value of the activation enthalpy, activation volume and stress dependence of activation volume. A plot of V_{ex} b^{-3} as a function of the σ/μ' at a strain of 0.5, for different temperatures is shown in Fig. 4(a). As is expected for thermally activated processes, here too, V_{ex} b^{-3} decreases with increasing σ/μ'. Fig. 4(b) shows the effect of strain on V_{ex} b^{-3} vs. σ/μ' at 1386 K. At the other temperatures too, the nature of variation of V b^{-3} vs. σ/μ' is similar. It is seen that for the higher stresses the activation volume is independent of strain, whereas for the lower stresses (lower strain rates), the activation volume varies with strain. The activation volumes at 0.4 and 0.5 strains are similar throughout. Note that this region of lower stress at 1380 K, is the region showing the highest strain rate sensitivity.

Activation enthalpy is a thermodynamic parameter quantifying the energy required to overcome barriers to deformation by thermal activation. Fig. 5 shows the contour plot of the experimental activation enthalpy (ΔH_{ex}) as a function of temperature and strain rate. In most of the strain rate and temperature space ΔH_{ex} varies little, remaining about 60–80 kJ mol^{-1}. In the range where m is 0.5 (1375 K, 0.0025 s^{-1}) the activation energy is about 90–100 kJ mol^{-1}.

Alternatively the stress, strain rate, and temperature can also be related through the following Arrhenius type kinetic equation

$$\dot{\varepsilon} = A\sigma^n \exp\left(\frac{-Q}{RT}\right), \tag{7a}$$

where Q is the activation energy, n is the stress exponent, and A is a constant. In a general case, Q and n are functions of any two of the three variables $\dot{\varepsilon}$, σ and T. For a special case within a domain of m, the variations

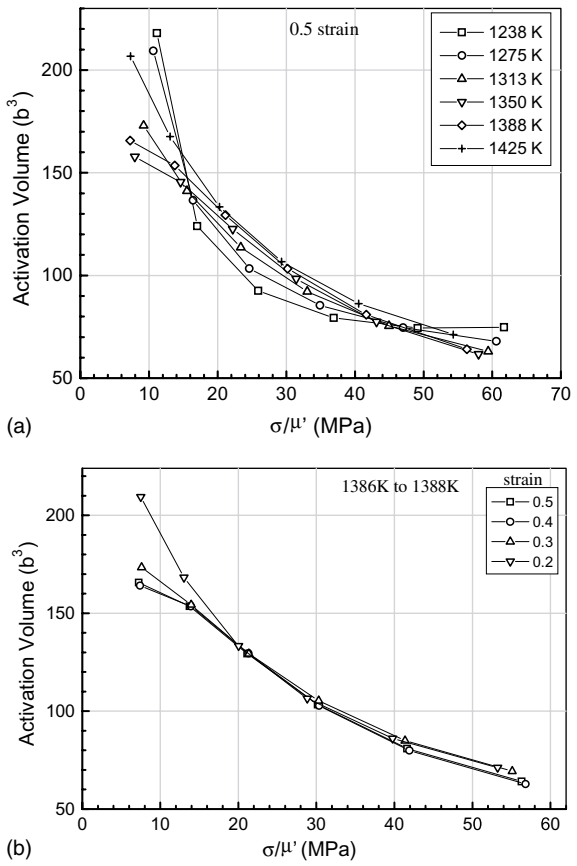

Fig. 4. (a) V_{ex} b^{-3} vs. σ/μ' for different temperatures at 0.5 strain, and (b) V_{ex} b^{-3} vs. σ/μ' for different strains for 1386 K.

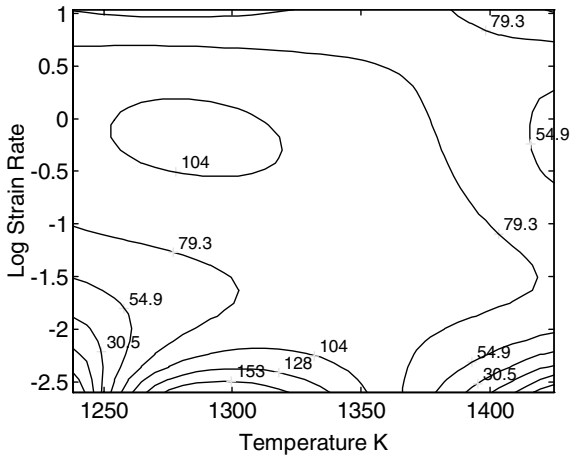

Fig. 5. Contour plot of ΔH_{ex} at 0.5 strain.

of n and Q with $\dot{\varepsilon}$ and T are ignored, and assumed constant. Eq. (7a) can be rewritten as

Table 2
A comparison of V_{ex}, Q, n and domain for Zr [13] and Zr–2.5Nb

	Zr–2.5Nb (this study)	Zr [13]
V_{ex} (b^3)	130–170	120–210
Q (no μ correction) (kJ mol b^3)	120	110
Q (μ correction) (kJ mol b^3)	70	80
n	3.2	2.7
Domain range	1350–1400 K 2×10^{-3} to 10^{-2} s^{-1}	1275–1320 K 10^{-3}–10^{-2} s^{-1}

$$\ln \sigma = \left(\frac{Q}{nR}\right)\frac{1}{T} + \left(\frac{1}{n}\right)\ln \dot{\varepsilon} - \left(\frac{1}{n}\ln A\right). \tag{7b}$$

For n, Q, R, and A as constants, this reduces to a linear equation of $\ln \sigma$ with two variables $\ln \dot{\varepsilon}$ and $1/T$. The activation energy is obtained from Eq. (7b) with and without correcting the flow stress for variation of shear modulus with temperature and is shown in Table 2. Table 2 also compares the values of V_{ex} and Q, as obtained from Eqs. (5a) and (7b), respectively, and n and domain range, for Zr [13] and Zr–2.5Nb in order to bring about the effect of Nb. It is seen from this table that the shear modulus correction results in a lower value of the activation energy. Similar observations on the lowering of Q by taking into account the shear modulus correction, were made in a β-titanium alloy [21].

3.3. Deformed microstructure

The optical micrograph of the starting microstructure of Zr–2.5Nb is shown in Fig. 6(a), which reveals the morphology of the β-transformed structure within equiaxed prior β grain boundaries. The average grain size before deformation was approximately 120 μm. When hot deformations are carried out within the bounds of the strain rate sensitivity domain, the grain structure of prior β was observed to be equiaxed. Fig. 6(b) shows the microstructure after deformation at 0.01 s^{-1} and 1375 K. Here it is seen that the grains are near equiaxed but not well defined, and the grain boundaries show a broken structure. The microstructure after deformation at 0.002 s^{-1} and 1375 K is shown in Fig. 6(c). Here the grains are slightly larger, have well defined grain boundaries and are equiaxed. In contrast to this when deformation was carried outside the range of the domain, the deformed grain structure was elongated, as seen in Fig. 6(d). The implications of the effect of deformation conditions on the observed grain structure will be considered in Section 4.

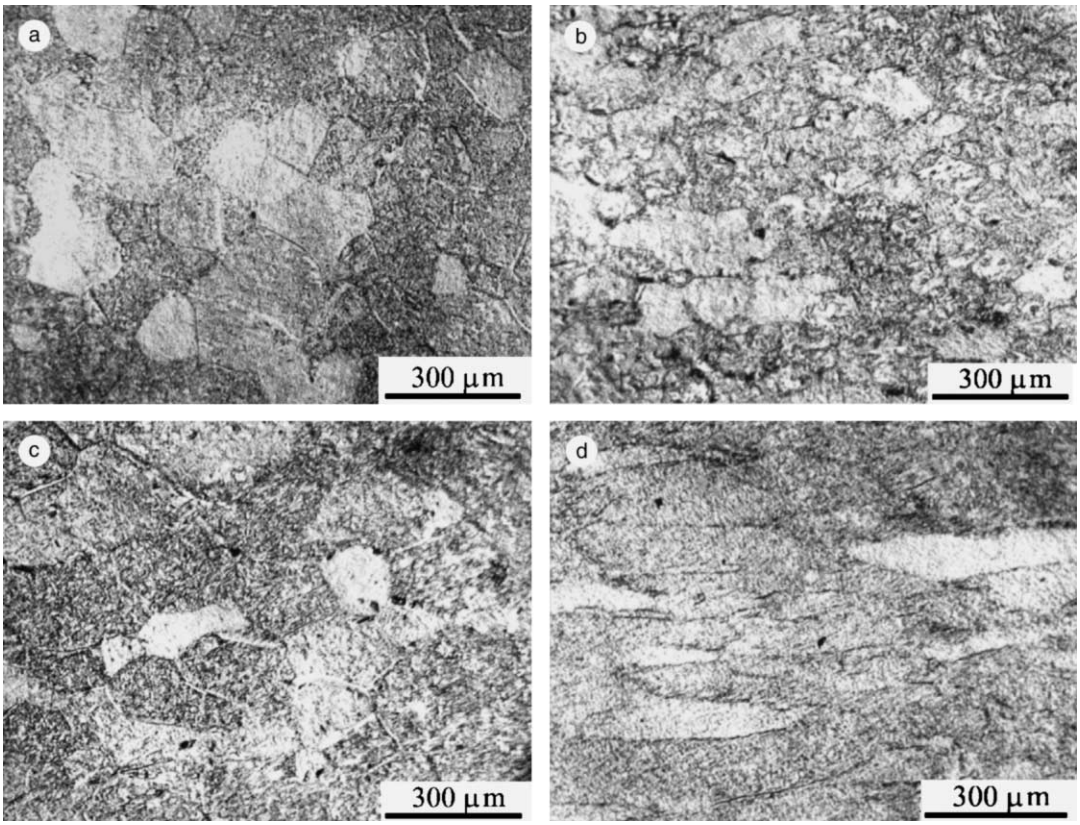

Fig. 6. (a) Microstructure of undeformed Zr–2.5Nb; (b) Zr–2.5Nb deformed at 0.01 s^{-1} and 1375 K; (c) Zr–2.5Nb deformed at 0.002 s^{-1} and 1375 K; (d) Zr–2.5Nb deformed at 5 s^{-1} and 1270 K.

4. Discussion

The domains observed in the processing maps are generally identified by correlating the strain rate sensitivity variations with temperature and strain rate on one hand and with those of ductility and the microstructural changes that occur in the deformed specimens on the other. This investigation has found that Zr–2.5Nb deformed in the β phase field shows a single domain with the following characteristic features:

(i) The domain occurs at a low strain rate of 10^{-3} s^{-1} and a high temperature of 1375 K.
(ii) The strain rate sensitivity is high (≈0.5) and its variation with strain rate is sharper in the domain than the rest of the regime of stable flow.
(iii) While the grain structure observed after deformation in this domain is equiaxed, the grain structure after deformation at higher strain rates and lower temperatures is elongated.

In addition to these, the stress–strain curves in this domain clearly show steady-state flow behaviour, as shown in Fig. 7. Further, the studies carried out by Rosinger and Unger [22] showed that in the β phase Zr–2.5%Nb exhibits a high ductility of about 150% at a strain rate of 10^{-3} s^{-1} and at temperatures greater than 1250 K. These observations and those of the present study suggest that Zr–2.5Nb deforms superplastically at low rates and high temperatures. Previously large grain size Zr and Ti alloys in the β phase have been shown to exhibit superplasticity [21,23,24], commonly referred to as large grain superplasticity (LGSP). This phenomenon of LGSP is usually associated with the formation of stable subgrains from the original large β grains, and is thought to result from the sliding on these subgrain boundaries with accomodation of the stresses generated at the subgrains triple junctions. At high temperatures, the β phase may accommodate these stress concentrations in the following ways: (1) diffusion aided dislocation processes, such as climb of edge dislocations, or non-conservative motion of jogged screw dislocations, (2) by processes such as dynamic recovery involving thermally activated cross slip, or thermal breaking of attractive junctions, and (3) by purely diffusional flow. LGSP has been reported in iron aluminides [25], where it has been suggested that

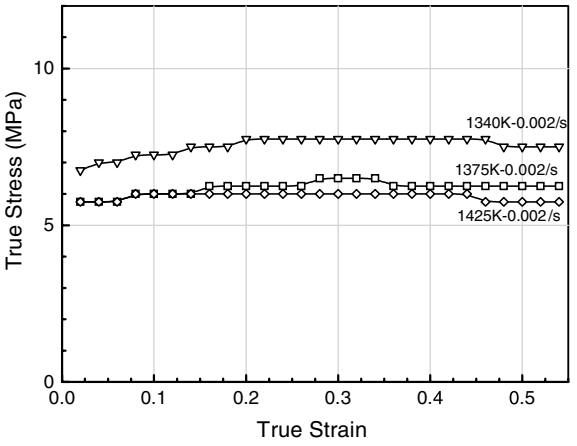

Fig. 7. Flow stress curves of Zr–2.5Nb within the strain rate sensitivity domain.

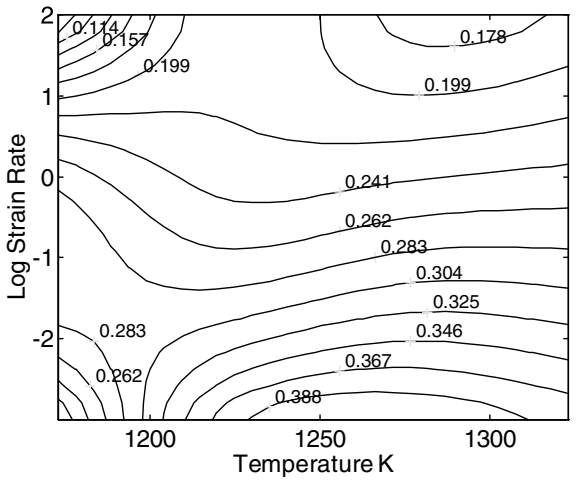

Fig. 8. Strain rate sensitivity contour plot with data taken from [13].

during high temperature deformation, dislocation arrays transform into subboundaries, which then slide and rotate accommodated by dislocation processes thereby resulting in superplastic flow.

In the present study the experimental activation volumes in the domain were observed to be about 150 b^3. These are considerably higher than those corresponding to dislocation climb ($V \sim 1\ b^3$) and lower than those for thermal breaking of attractive junctions ($V \sim 10^2$–$10^4\ b^3$) [3,19,26]. Thus both climb and the thermal breaking of attractive junctions can be ruled out as accommodation mechanisms during LGSP. The activation energy, Q, was obtained as 120 kJ mol^{-1} (without shear modulus correction) and 70 kJ mol^{-1} (with shear modulus correction), while the experimental activation enthalpy, ΔH_{ex}, as obtained from Eq. (5b), was found to range from 70 to 100 kJ mol^{-1} in the domain under consideration. The range of activation energies obtained are similar in magnitude as that for diffusion and definitely not higher than that for self diffusion in β Zr (~110 kJ mol^{-1}) [27]. The magnitude of the activation energy associated with the process of cross-slip in β Ti has generally been observed to be much higher than that for self-diffusion [28,29]. Considering that β Zr–2.5Nb behaves similarly, it can be inferred from the activation energy values that cross-slip is not the rate controlling accommodation process.

It is believed that LGSP involves a diffusional process where the subgrain boundaries act as source and sink for vacancies. The energy associated with these boundaries is influenced by the movement of jogs and their spacing, which in turn is controlled by the emission or absorption of vacancies [30,31]. If jogged screw dislocations are rate controlling, the activation energy will then equal that of either bulk or core diffusion. The observed activation energy values match those of the diffusional processes mentioned above, and the observed activation volume falls well within the range expected due to the motion of jogged dislocation (10–1000 b^3) [3,19,26]. Thus it may be concluded that the accommodation process involved in LGSP of β Zr–2.5Nb is controlled by the non-conservative jog motion of screw dislocations.

A comparison of the processing map obtained for β Zr reported earlier [13], with that of Zr–2.5Nb reported here, reveals that the maps are nearly the same. Fig. 8 shows the reconstructed strain rate sensitivity map of Zr (data taken from [13]). Comparing Figs. 3(b) and 8, the peak strain rate sensitivity in Zr–2.5Nb as compared to Zr is shifted to higher temperatures. The activation parameters recorded in Table 2 show that the accommodation processes in these materials are similar. The addition of Nb to Zr has been found to lower the diffusivity in the β phase [27] and is expected to induce solute drag effects in view of its smaller size as compared to Zr. Both these factors may be responsible for increasing the temperature where the peak strain rate sensitivity occurs.

5. Conclusions

The strain rate sensitivity map for Zr–2.5Nb in the β phase shows a domain in the temperature range of 1350–1400 K and the strain rate range of 0.002 and 0.01 s^{-1}. The optimum hot working condition is 1375 K and 0.002 s^{-1}, where the peak strain rate sensitivity of 0.5 occurs. A high strain rate sensitivity and the observation of large equiaxed grains in this domain, suggest the occurrence of large grain superplasticity. In contrast, deformation at lower temperatures and higher strain rates result in elongated grains. From the experimental activation enthalpy and activation volume calculations it is suggested that the accommodation mechanism during

large grain superplasticity in β Zr–2.5Nb is the non-conservative movement of jogged dislocations. Addition of Nb does not affect the deformation characteristics significantly, but does shift the peak strain rate domain to higher temperatures.

Acknowledgements

The authors are grateful to Dr S. Banerjee, Director Materials Group, and Dr P.K. De, Head Materials Science Section, for taking keen interest in this program. Special thanks are due to Mr P.J. Potdar for his useful suggestions and help during experimentation. The authors deeply regret the sudden demise of their coworker, Mr Lalit Kumar, whose involvement was critical during the initial stages of this work.

References

[1] M.J. Lutton, J.J. Jonas, Can. Metall. Quart. 11 (1972) 79.
[2] D.J. Abson, J.J. Jonas, J. Nucl. Mater. 42 (1973) 73.
[3] B.N. Meherotra, K. Tangri, Acta Metall. 28 (1980) 1385.
[4] A.M. Garde, H.M. Chung, T.F. Kassner, Acta Metall. 26 (1978) 153.
[5] R. Choubey, J.J. Jonas, Metal Sci. 15 (1981) 30.
[6] J.K. Chakravartty, Y.V.R.K. Prasad, M.K. Asundi, Metall. Trans. 22A (1991) 829.
[7] J.K. Chakravartty, S. Banerjee, Y.V.R.K. Prasad, M.K. Asundi, J. Nucl. Mater. 187 (1992) 260.
[8] J.K. Chakravartty, Y.V.R.K. Prasad, M.K. Asundi, in: Proceedings of 9th International Symposium on Zirconium in Nuclear Industry 1992, ASTM STP 1132, ASTM, Philadelphia, PA, p. 44.
[9] J.K. Chakravartty, G.K. Dey, S. Banerjee, Y.V.R.K. Prasad, J. Nucl. Mater. 218 (1995) 247.
[10] J.K. Chakravartty, G.K. Dey, S. Banerjee, Y.V.R.K. Prasad, Mater. Sci. Technol. 12 (1996) 705.
[11] H.E. Rosinger, P.C. Bera, W.R. Clendening, J. Nucl. Mater. 82 (1979) 286.
[12] J.J. Jonas, B. Heritier, M.J. Luton, Metall. Trans. 10A (1979) 611.
[13] J.K. Chakravartty, S. Banerjee, Y.V.R.K. Prasad, Scr. Metall. Mater. 26 (1992) 75.
[14] H.L. Gegel, J.C. Malas, S.M. Doraivelu, V.A. Shende, in: Metals Hand Book, vol. 14, American Society of Metals, Metals Park, OH, 1987, p. 417.
[15] J.C. Malas, V. Seetharaman, J. Metall. 44 (1992) 8.
[16] J.M. Alexander, in: J.G. Lenard (Ed.), Modelling of Hot Deformation of Steels, Spring, Berlin, 1989, p. 101.
[17] I. Philippart, H.J. Rack, Mater. Sci. Eng. A 254 (1998) 253.
[18] A. Padel, A. Groff, J. Nucl. Mater. 59 (1976) 325.
[19] A.G. Evans, R.D. Rawlings, Phys. Status Solidi 34 (1969) 9.
[20] H. Conrad, J. Metals 16 (1964) 582.
[21] G.C. Morgan, C. Hammond, Mater. Sci. Eng. 86 (1987) 159.
[22] H.E. Rosinger, A.E. Unger, Superplastic and strain rate dependent plastic flow of Zr–2.5Nb between 873 and 1373 K, AECL-6418, Atomic Energy Canada, Pinawa, Manitoba, 1979.
[23] P. Griffiths, C. Hammond, Acta Metall. 20 (1972) 935.
[24] V.V. Balasubrahmanyam, Y.V.R.K. Prasad, Mater. Sci. Technol. 17 (2001) 1222.
[25] T.G. Nieh, J. Wadsworth, Inter. Metals Rev. 44 (2) (1999) 59.
[26] E.A. Little, J. Aust. Inst. Metals 21 (1976) 50.
[27] D.L. Douglass, Physical Metallurgy of Zirconium, Atomic Energy Review, IAEA, Vienna, Austria, 1971.
[28] T. Seshacharyulu, S.C. Medeiros, W.G. Frazier, Y.V.R.K. Prasad, Mater. Sci. Eng. A 284 (2000) 184.
[29] D.G. Robertson, H.B. McShane, Mater. Sci. Technol. 14 (1998) 339.
[30] J. Weertman, Trans. ASM 61 (1968) 681.
[31] H. Glieter, Acta Metall. 27 (1979) 187.